Electronic Supplementary Information

Electronic Structure Modification of Metal Phthalocyanines by Carbon Nanotube Support for Efficient Oxygen Reduction to Hydrogen Peroxide

Yesol Lee,‡[a] Chaehyeon Lee,‡[b] Seoin Back,*[b] and Young Jin Sa*[a]

[a]Department of Chemistry, Kwangwoon University, Seoul 01897, Republic of Korea.

[b]Department of Chemical and Biomolecular Engineering, Institute of Emergent Materials, Sogang University, Seoul 04107, Republic of Korea.

Corresponding Authors

*E-mail: youngjinsa@kw.ac.kr (Y.J.S.); sback@sogang.ac.kr (S.B.)

‡These authors contributed equally to this work.

Supplementary Figures and Tables

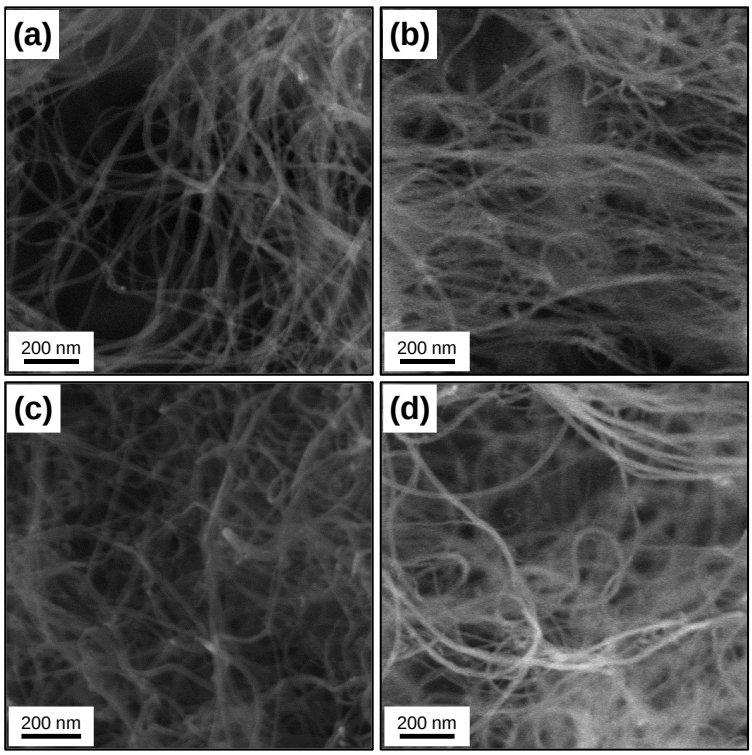

Fig. S1. SEM images of (a) CNT, (b) CoPc/CNT, (c) MnPc/CNT, and (d) FePc/CNT.

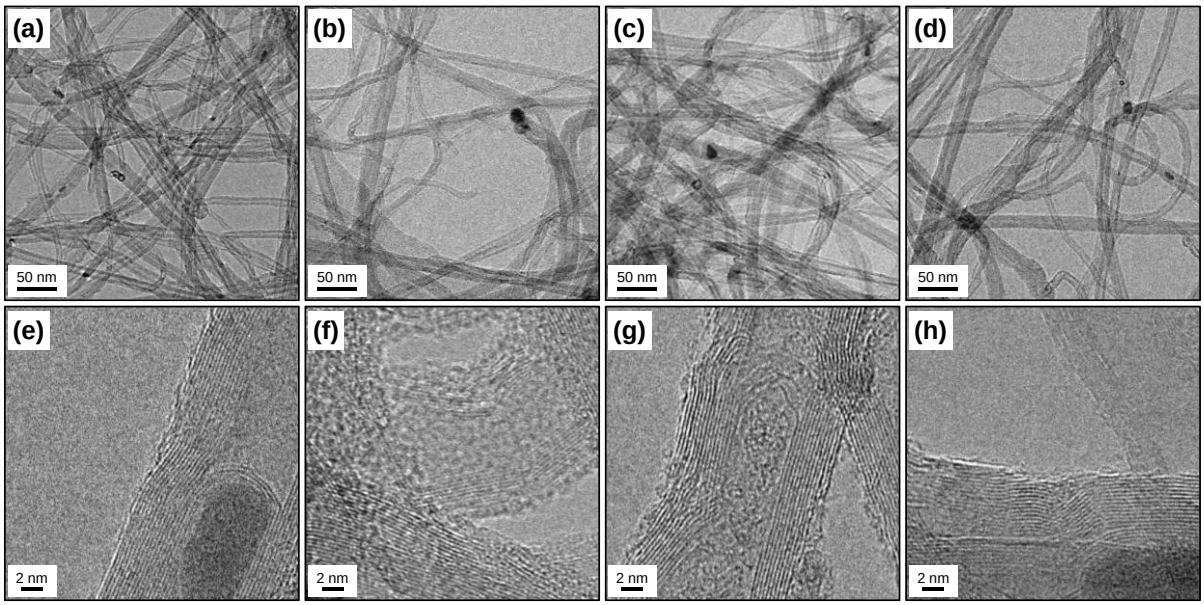

Fig. S2. TEM images of (a) CNT, (b) CoPc/CNT, (c) MnPc/CNT, and (d) FePc/CNT, and high-resolution TEM images of (e) CNT, (f) CoPc/CNT, (g) MnPc/CNT, and (h) FePc/CNT.

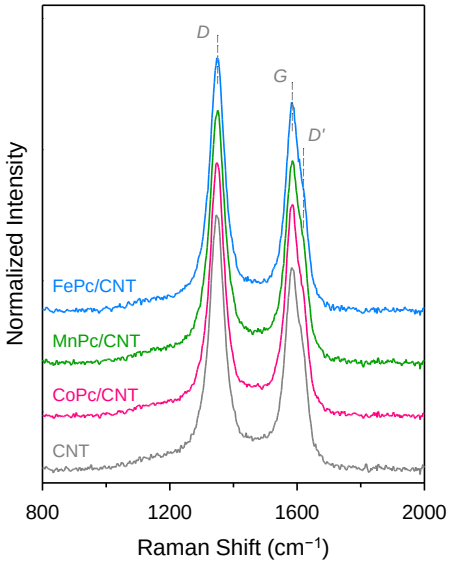

Fig. S3. Raman spectra of CNT, CoPc/CNT, MnPc/CNT, and FePc/CNT.

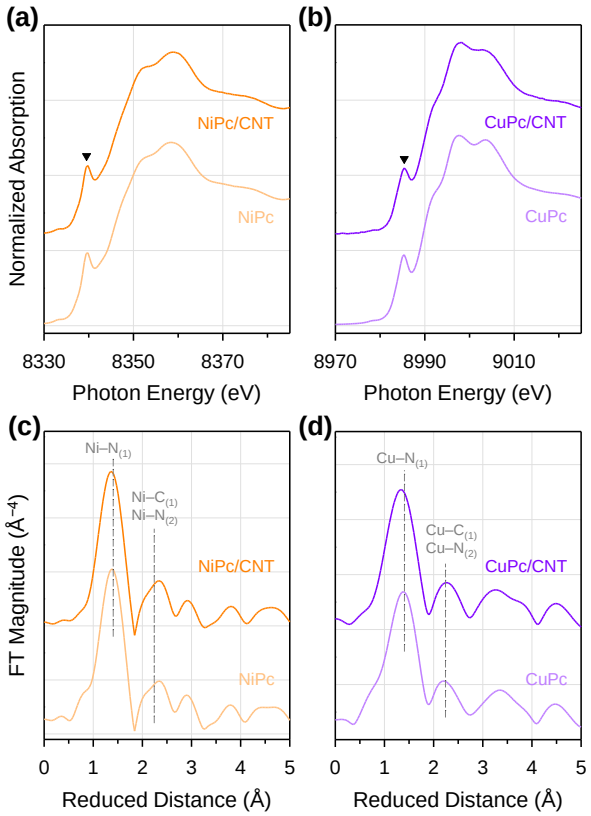

Fig. S4. (a) Ni *K*-edge XANES spectra of NiPc/CNT and NiPc and (b) Cu *K*-edge XANES spectra of CuPc/CNT and CuPc. The inverted triangle indicates the pre-edge peak for D_{4h} symmetry. Radial distribution functions obtained from Fourier transform of k^3-weighted EXAFS spectra of (c) NiPc/CNT and NiPc and (d) CuPc/CNT and CuPc.

Table S1. ICP-MS results for MPc/CNT.

Catalyst	M (ppm)	MPc (wt%)
CoPc/CNT	2560	2.5
FePc/CNT	3670 (1920 from CNT)	1.8
MnPc/CNT	2180	2.3
NiPc/CNT	2330	2.3
CuPc/CNT	1970	1.8
CNT	1920	-

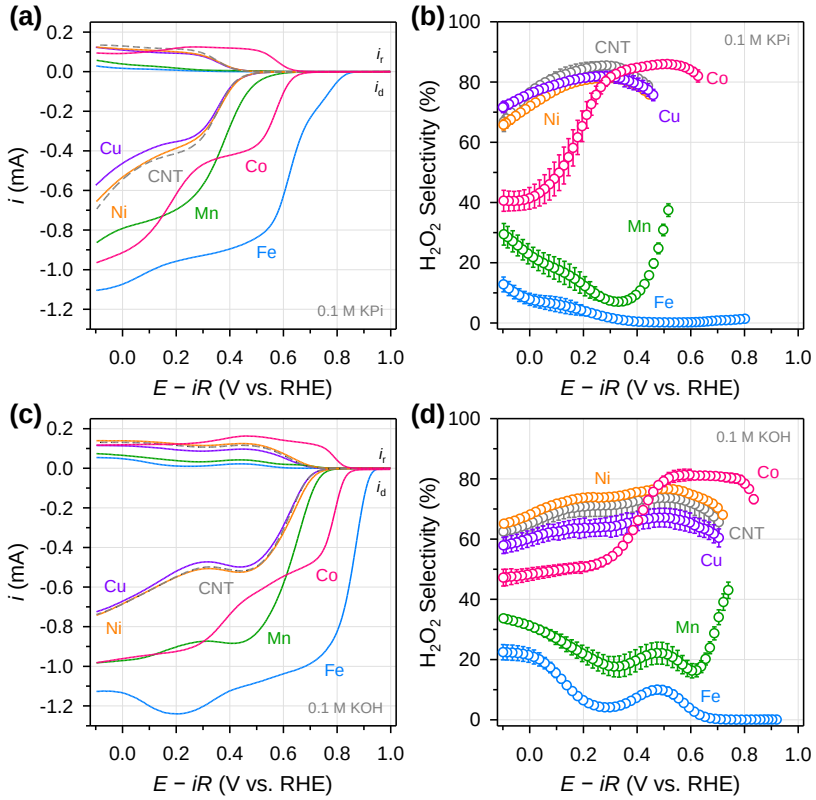

Fig. S5. (a) RRDE voltammograms of MPc/CNT measured in O_2-saturated 0.1 M KPi (pH 8) and (b) the corresponding H_2O_2 selectivity calculated from the RRDE analysis. (c) RRDE voltammograms of MPc/CNT measured in O_2-saturated 0.1 M KOH and (d) the corresponding H_2O_2 selectivity calculated from the RRDE analysis.

Table S2. Summary of ORR onset potentials of MPc/CNT and MPc in 0.1 M KPi (pH 8) and 0.1 M KOH. The onset potential was defined at the potential where the current density of 50 μg cm^{-2} was obtained.

Catalyst	E_{onset} **(V vs. RHE) in 0.1 M KPi (pH 8)**	E_{onset} **(V vs. RHE) in 0.1 M KOH**
CoPc/CNT	0.663 ± 0.003	0.861 ± 0.002
CoPc	0.497 ± 0.038	0.800 ± 0.019
FePc/CNT	0.835 ± 0.004	0.938 ± 0.002
FePc	0.577 ± 0.110	0.886 ± 0.002
MnPc/CNT	0.576 ± 0.016	0.768 ± 0.004
MnPc	0.334 ± 0.025	0.715 ± 0.002
NiPc/CNT	0.479 ± 0.002	0.750 ± 0.003
NiPc	0.308 ± 0.012	0.724 ± 0.003
CuPc/CNT	0.483 ± 0.008	0.733 ± 0.006
CuPc	0.288 ± 0.031	0.717 ± 0.007
CNT	0.476 ± 0.015	0.732 ± 0.002

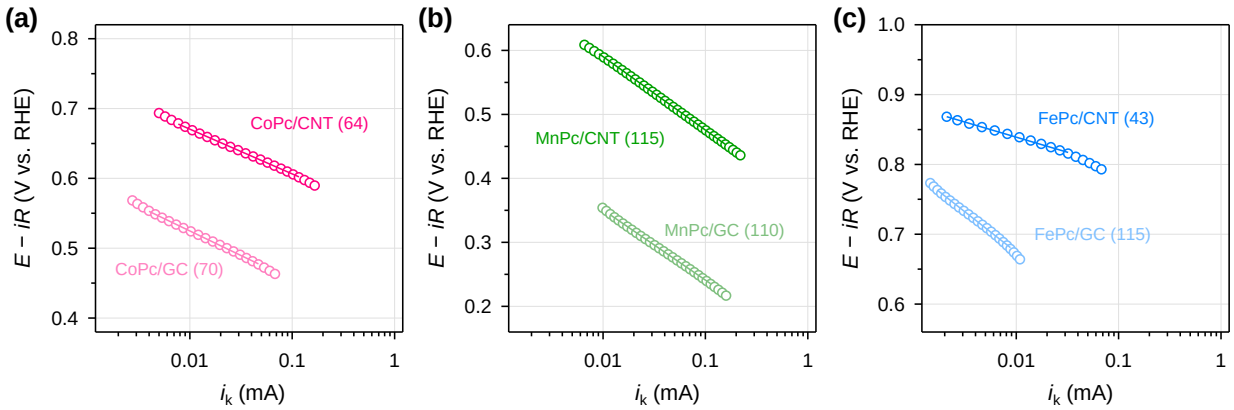

Fig. S6. Tafel plots for (a) CoPc/CNT and CoPc/GC, (b) MnPc/CNT and MnPc/GC, and (c) FePc/CNT and FePc/GC measured in 0.1 M KPi (pH 8). The numbers in the parenthesis indicate the Tafel slopes in mV dec^{-1}.

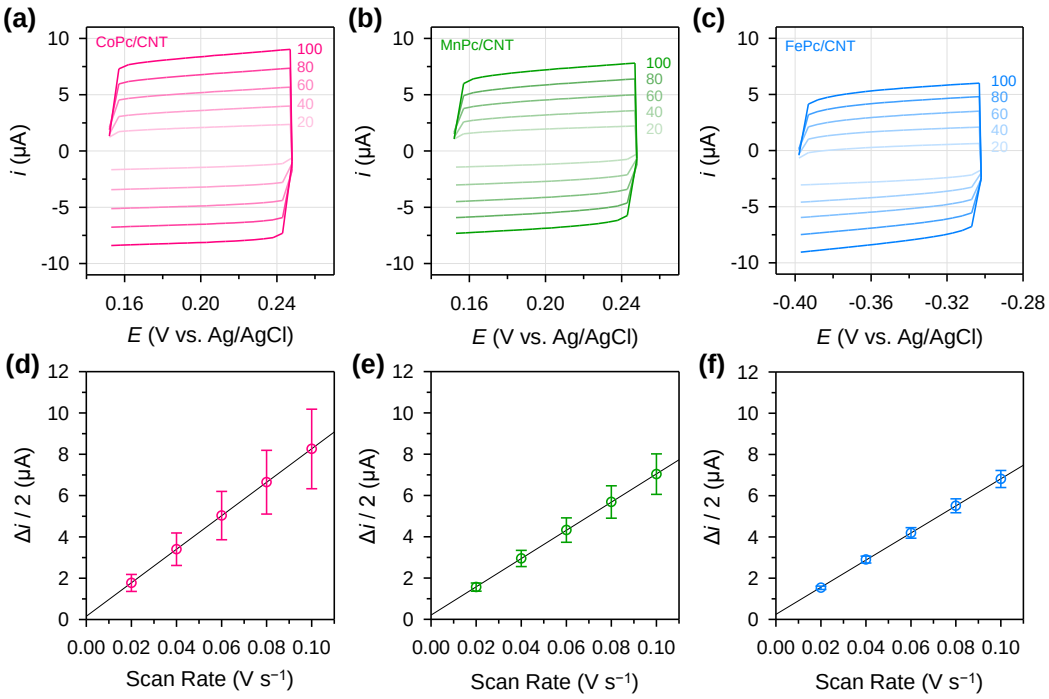

Fig. S7. Cyclic voltammetry (CV) curves of (a) CoPc/CNT, (b) MnPc/CNT, and (c) FePc/CNT measured in N_2-saturated 0.1 M KPi (pH 8) at different potential scan rates. The numbers indicate the scan rates in mV s^{-1}. The half of the height of the CV curve as a function of the scan rates for (d) CoPc/CNT, (e) MnPc/CNT, and (f) FePc/CNT. The slope corresponds to the double layer capacitance summarized in **Table S3**.

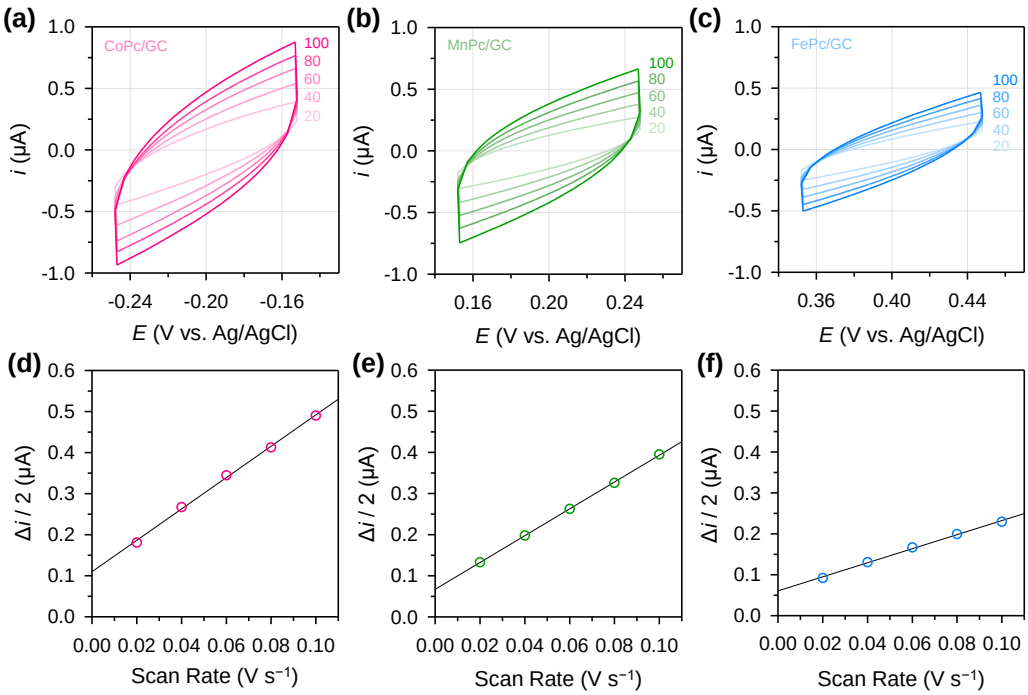

Fig. S8. CV curves of (a) CoPc/GC, (b) MnPc/GC, and (c) FePc/GC measured in N_2-saturated 0.1 M KPi (pH 8) at different potential scan rates. The numbers indicate the scan rates in mV s^{-1}. The half of the height of the CV curve as a function of the scan rates for (d) CoPc/GC, (e) MnPc/GC, and (f) FePc/GC. The slope corresponds to the double layer capacitance summarized in **Table S3**.

Table S3. Summary of double layer capacitance (C_{dl}) and electrochemically active surface area (ECSA) of MPc/CNT and MPc/GC obtained from the CV analysis at different scan rates in 0.1 M KPi (pH 8) and 0.1 M KOH electrolytes. Specific capacitance of 20 μF cm^{-2}_{cat} was used to calculate ECSA from C_{dl}.

Catalyst	**C_{dl} (μF) 0.1 M KPi**	**ECSA (cm^2_{cat}) 0.1 M KPi**	**C_{dl} (μF) 0.1 M KOH**	**ECSA (cm^2_{cat}) 0.1 M KOH**
CoPc/CNT	81.1	4.1	83.8	4.2
CoPc	3.82	0.19	4.75	0.24
MnPc/CNT	68.4	3.4	85.4	4.3
MnPc	3.26	0.16	10.0	0.50
FePc/CNT	65.8	3.3	109.6	5.5
FePc	1.72	0.09	7.45	0.37

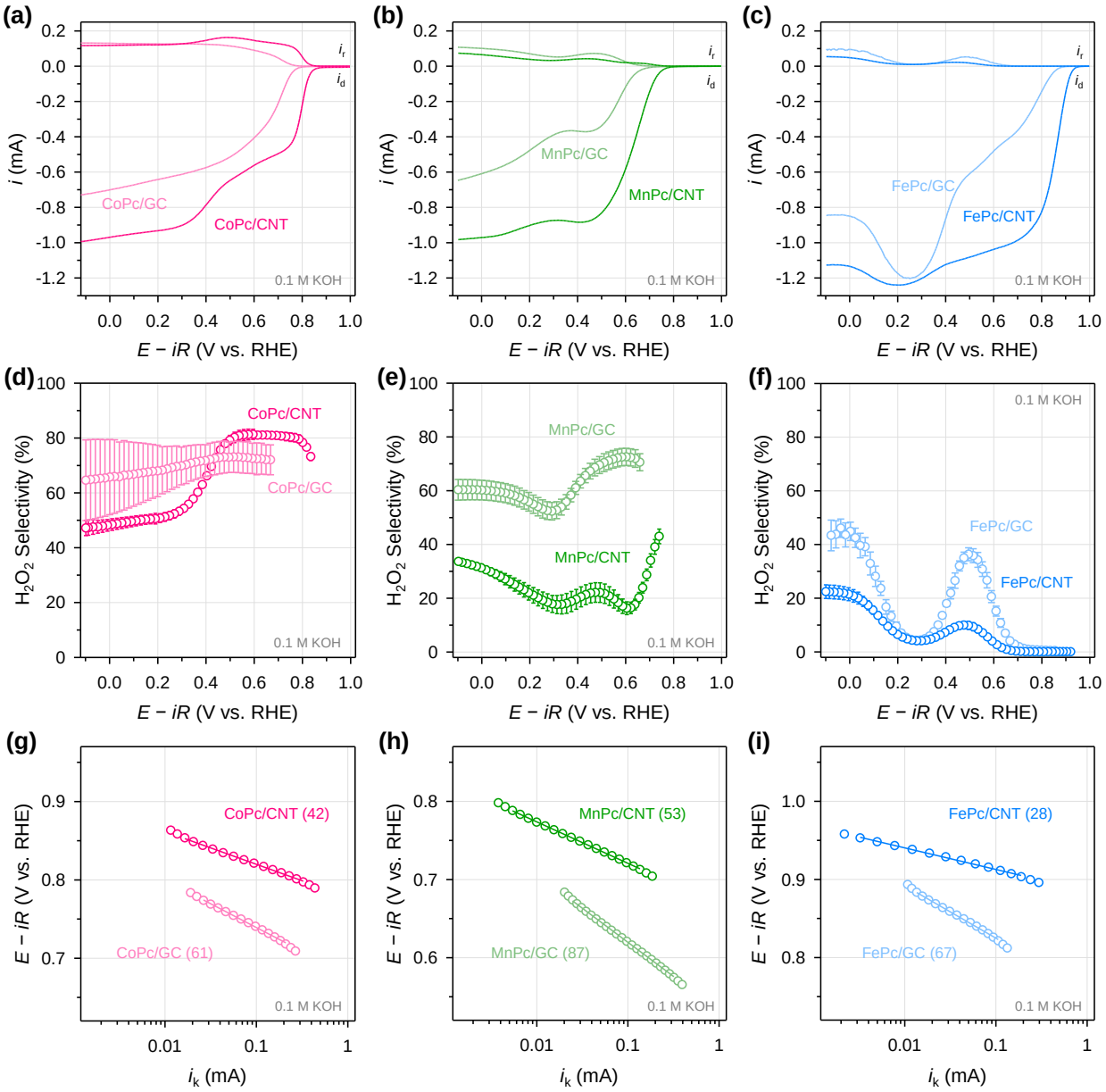

Fig. S9. RRDE voltammograms of (a) CoPc/CNT and CoPc/GC, (b) MnPc/CNT and MnPc/GC, and (c) FePc/CNT and FePc/GC measured in O_2-saturated 0.1 M KOH at an electrode rotation speed of 1600 rpm. H_2O_2 selectivity of (d) CoPc/CNT and CoPc/GC, (e) MnPc/CNT and MnPc/GC, and (f) FePc/CNT and FePc/GC calculated from the RRDE analysis. Tafel plots for (g) CoPc/CNT and CoPc/GC, (h) MnPc/CNT and MnPc/GC, and (i) FePc/CNT and FePc/GC. The numbers in the parenthesis indicate the Tafel slopes in mV dec^{-1}.

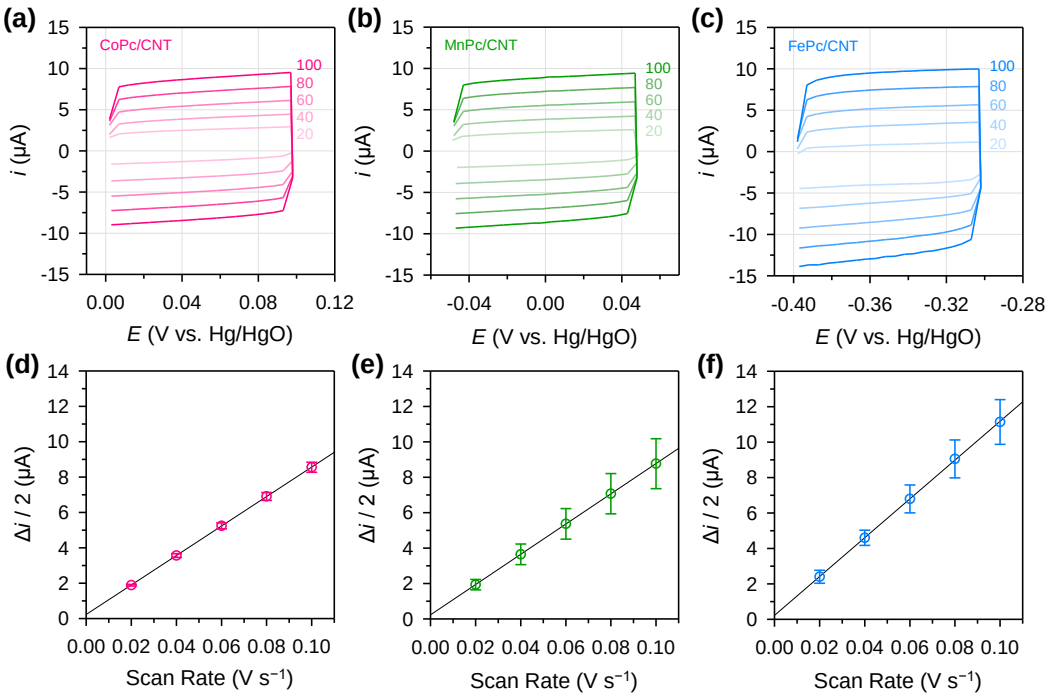

Fig. S10. CV curves of (a) CoPc/CNT, (b) MnPc/CNT, and (c) FePc/CNT measured in N_2-saturated 0.1 M KOH at different potential scan rates. The numbers indicate the scan rates in mV s^{-1}. The half of the height of the CV curve as a function of the scan rates for (d) CoPc/CNT, (e) MnPc/CNT, and (f) FePc/CNT. The slope corresponds to the double layer capacitance summarized in **Table S3**.

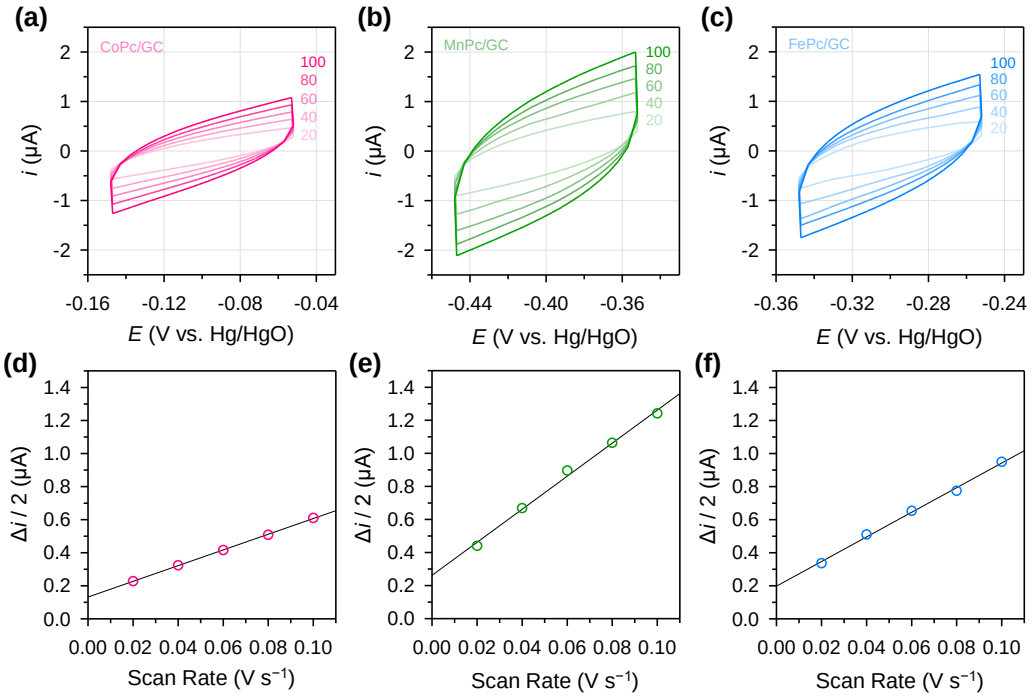

Fig. S11. CV curves of (a) CoPc/GC, (b) MnPc/GC, and (c) FePc/GC measured in N_2-saturated 0.1 M KOH at different potential scan rates. The numbers indicate the scan rates in mV s^{-1}. The half of the height of the CV curve as a function of the scan rates for (d) CoPc/GC, (e) MnPc/GC, and (f) FePc/GC. The slope corresponds to the double layer capacitance summarized in **Table S3**.

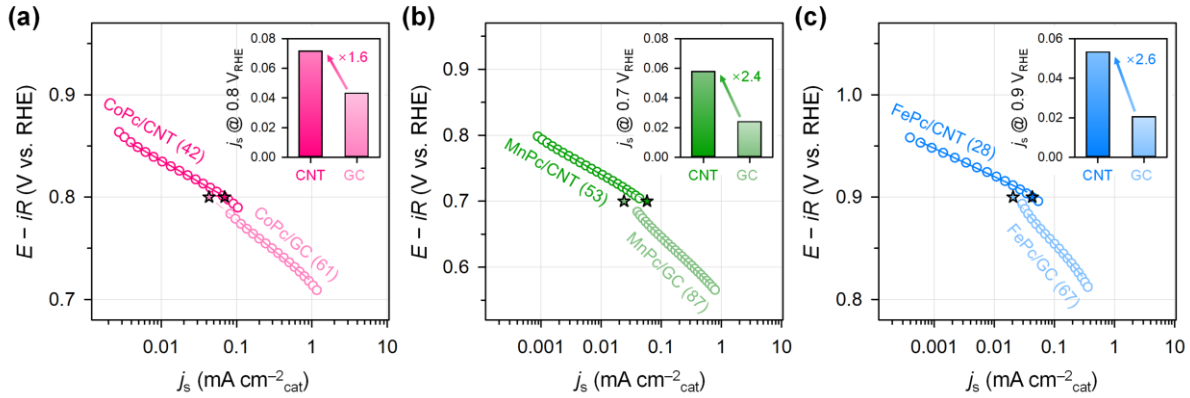

Fig. S12. ECSA-normalized specific activity of (a) CoPc/CNT and CoPc/GC, (b) MnPc/CNT and MnPc/GC, and (c) FePc/CNT and FePc/GC in 0.1 M KOH. Inset of (a)–(c) represents a bar graph comparing the specific activity of MPc molecules with and without the CNT support at a potential near the kinetic region. Dotted line and star symbol denote the Tafel extrapolation lines and the specific activity at each potential, respectively. The numbers in the parenthesis indicate the Tafel slopes in mV dec^{-1}.

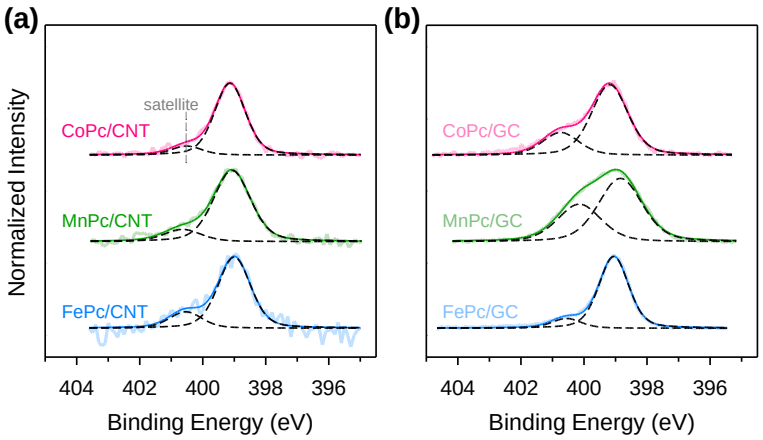

Fig. S13. N 1s XPS spectra and deconvoluted peaks of (a) CoPc/CNT, MnPc/CNT, and FePc/CNT and (b) CoPc/GC, MnPc/GC, and FePc/GC.

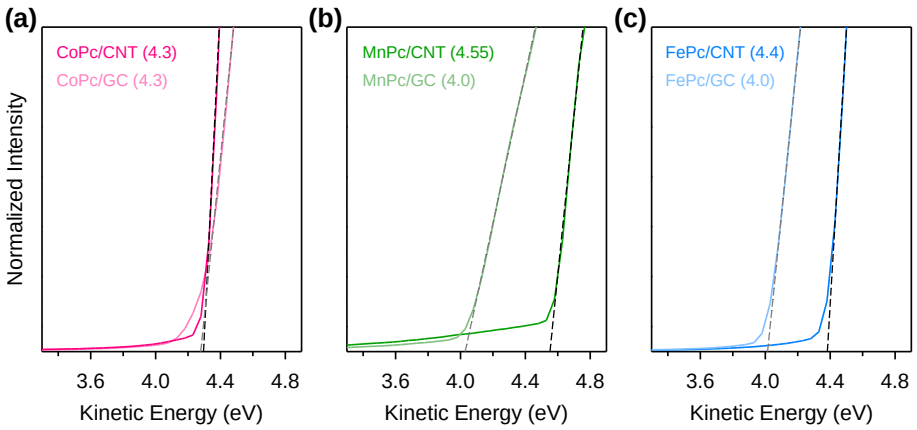

Fig. S14. UPS spectra of (a) CoPc/CNT and CoPc/GC, (b) MnPc/CNT and MnPc/GC, and (c) FePc/CNT and FePc/GC at the secondary electron cutoff region. The numbers in the parenthesis indicate the work function values in eV.

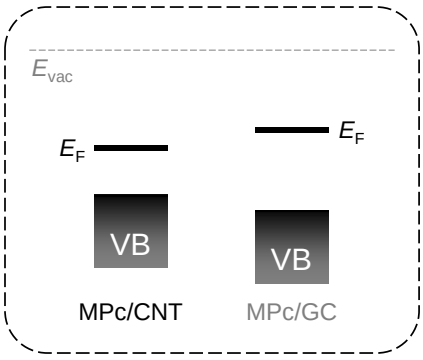

Fig. S15. Schematic illustration of the energy states at the valence band region for MPc/CNT and MPc/GC.

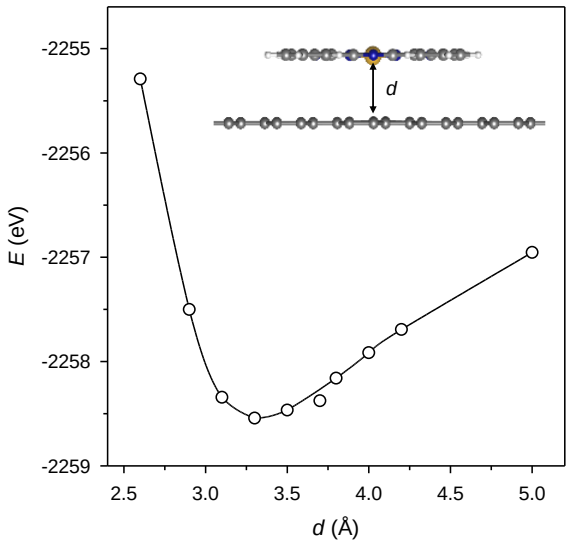

Fig. S16. The calculated total DFT energy of MPc/CNT as a function of the interlayer distance, *d*.

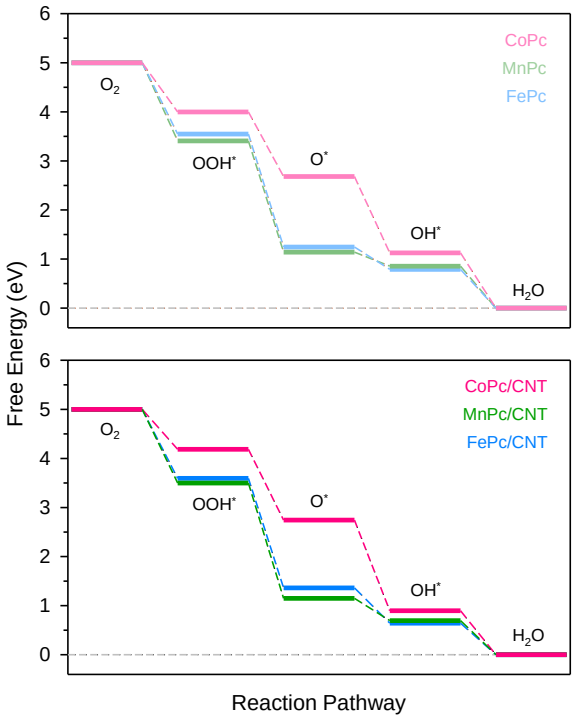

Fig. S17. Free-energy diagram of ORR on MPc (upper plot) and MPc/CNT (lower plot) (M = Co, Mn, and Fe) at 0 V (vs. RHE).

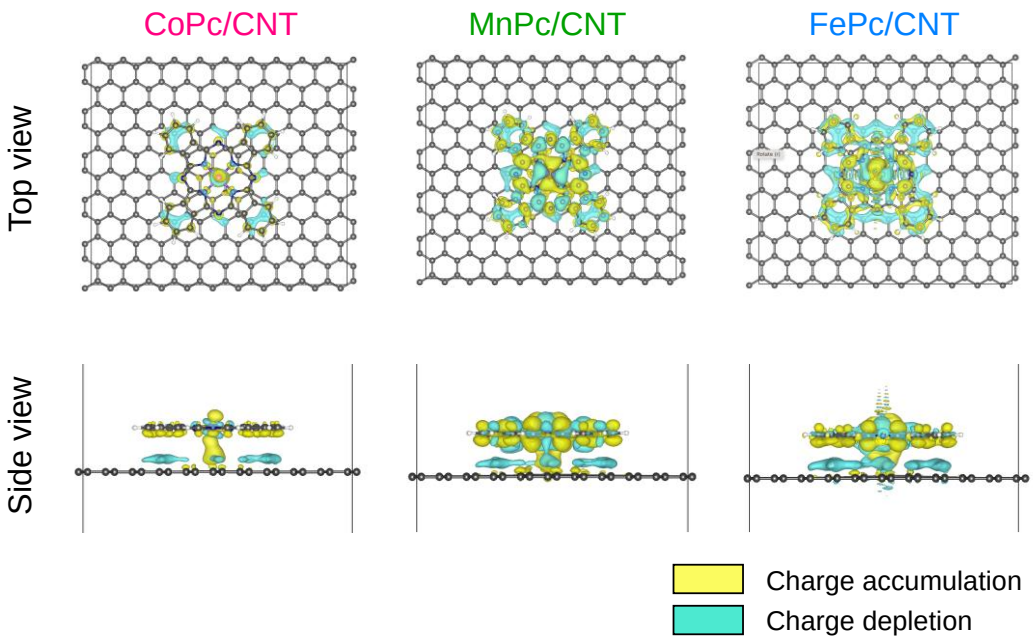

Fig. S18. The charge density difference (CDD) of MPc/CNT with an isosurface value of 0.002 e/Å^3. CDD is calculated as $\Delta\rho = \rho_{total} - \rho_{MPc} - \rho_{CNT}$, where ρ_{total}, ρ_{MPc}, and ρ_{CNT} are charge densities of total system, MPc molecule and CNT support, respectively. The yellow and blue color represent charge accumulation and charge depletion, respectively.

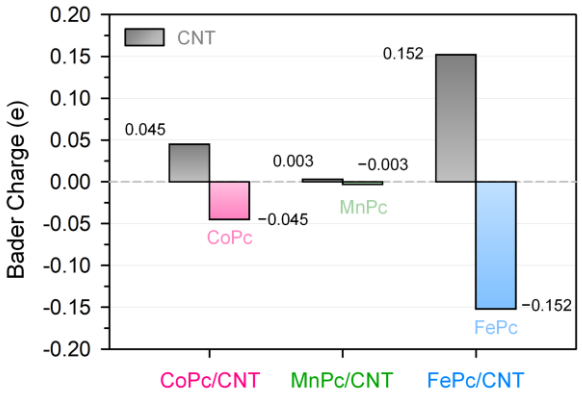

Fig. S19. Bader charge analysis of MPc/CNT. The gray and colored bars represent the total Bader charge of CNT and MPc in MPc/CNT, respectively. More positive charge indicates more oxidized states. Thus, the positive Bader charge of CNT indicates that electron transfer is from CNT to MPc.

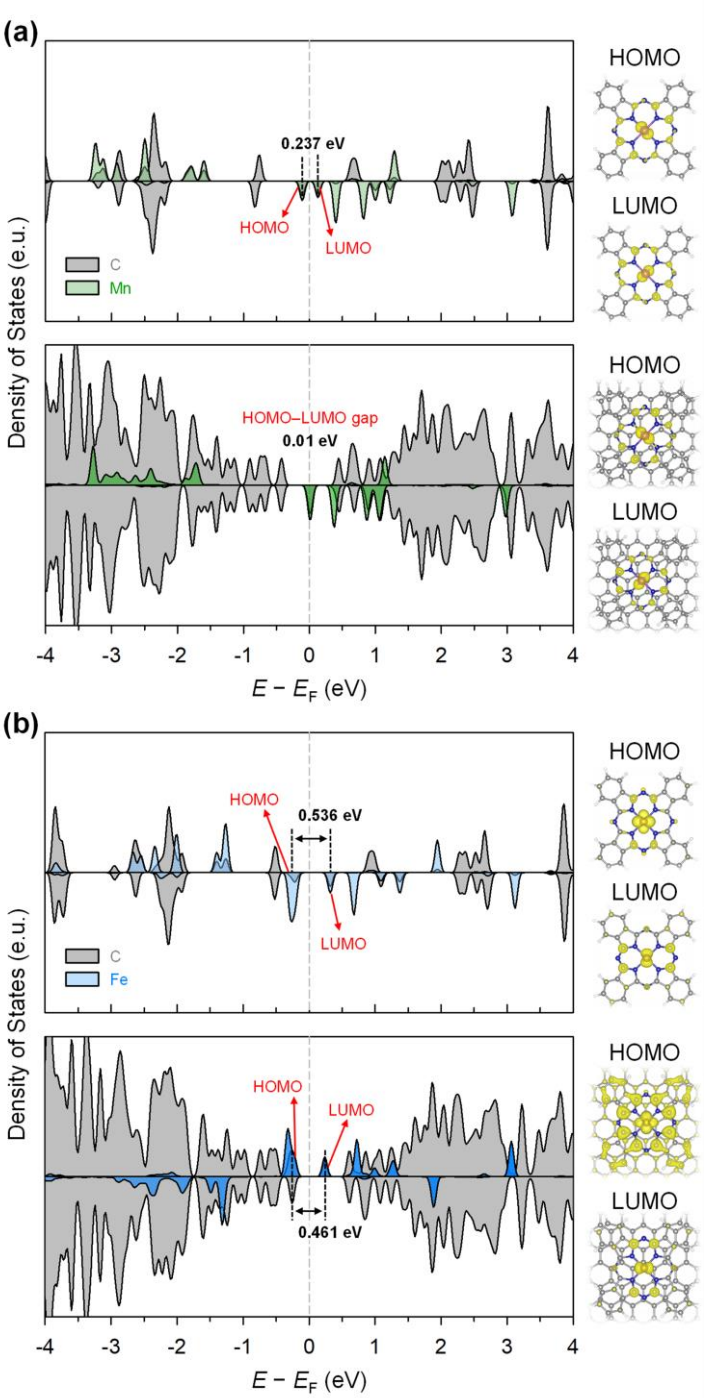

Fig. S20. Partial density of states (PDOS) of MPc and MPc/CNT for (a) Mn and (b) Fe. Electron density distributions of HOMO and LUMO are illustrated with an isosurface level of 0.002 e/Å^3.

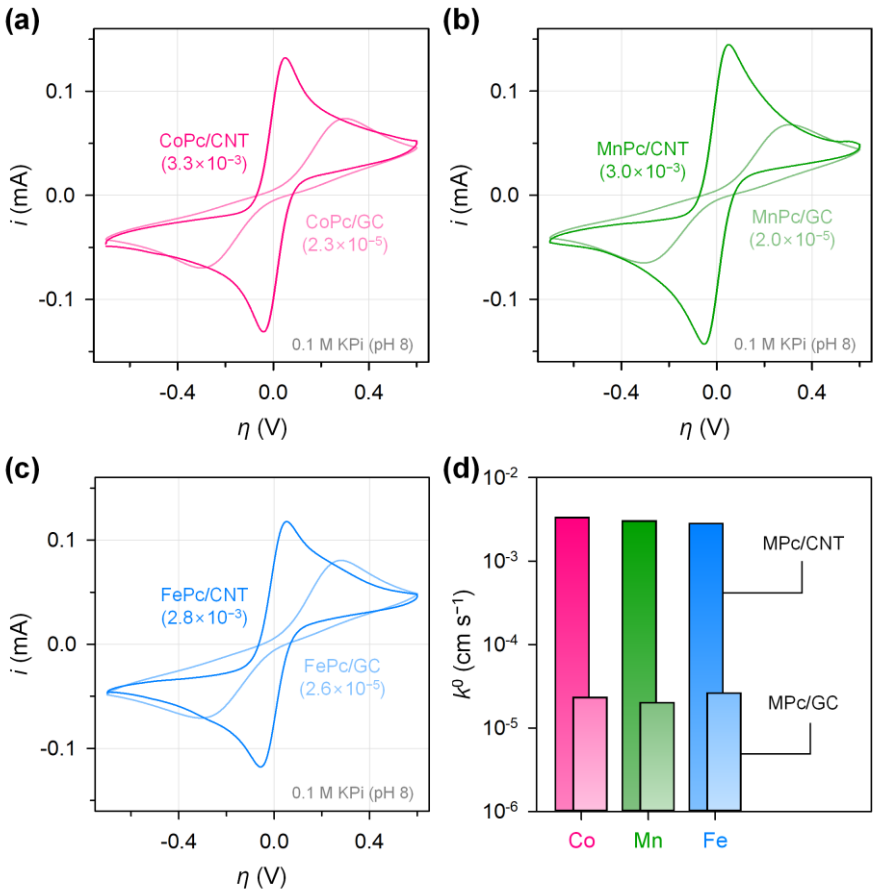

Fig. S21. CV curves of (a) CoPc/CNT and CoPc/GC, (b) MnPc/CNT and MnPc/GC, and (c) FePc/CNT and FePc/GC measured in 0.1 M KPi (pH 8) containing 2 mM $K_3[Fe(CN)_6]$ + 2 mM $K_4[Fe(CN)_6]$ at a scan rate of 100 mV s^{-1}. The numbers in the parenthesis indicate the heterogeneous electron transfer (ET) rate constant (k^0) in cm s^{-1}. (d) The bar graph showing the k^0 values of the MPc/CNT catalysts.

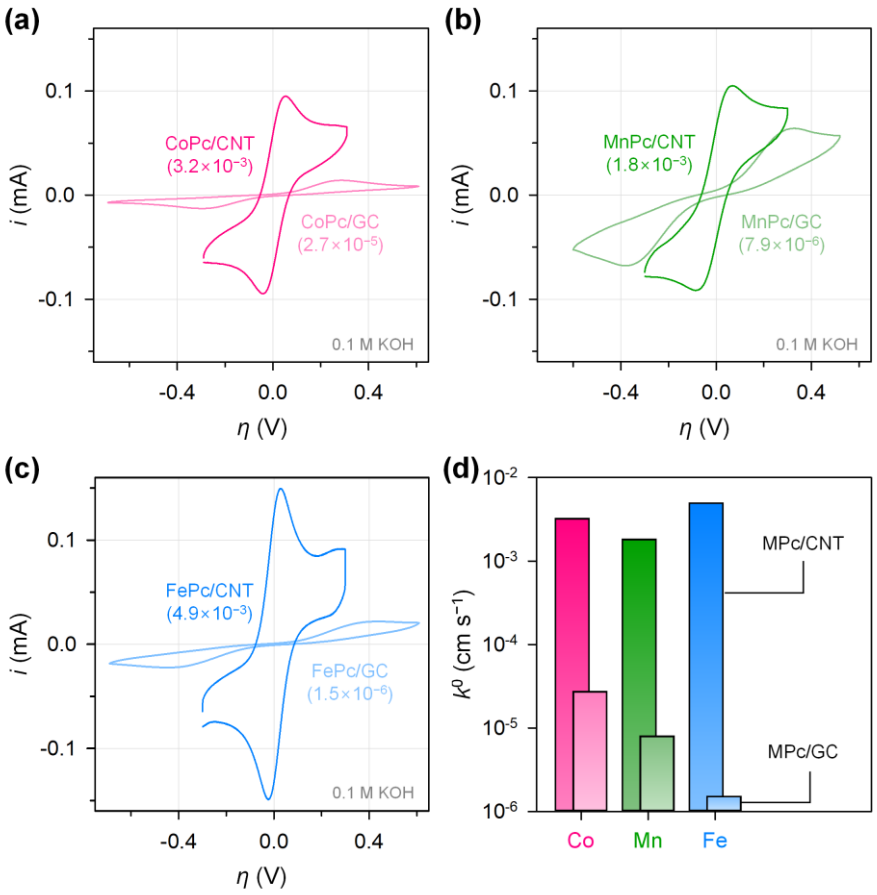

Fig. S22. CV curves of (a) CoPc/CNT and CoPc/GC, (b) MnPc/CNT and MnPc/GC, and (c) FePc/CNT and FePc/GC measured in 0.1 M KOH containing 2 mM $K_3[Fe(CN)_6]$ + 2 mM $K_4[Fe(CN)_6]$ at a scan rate of 100 mV s^{-1}. The numbers in the parenthesis indicate the heterogeneous ET rate constant (k^0) in cm s^{-1}. (d) The bar graph showing the k^0 values of the MPc/CNT catalysts.

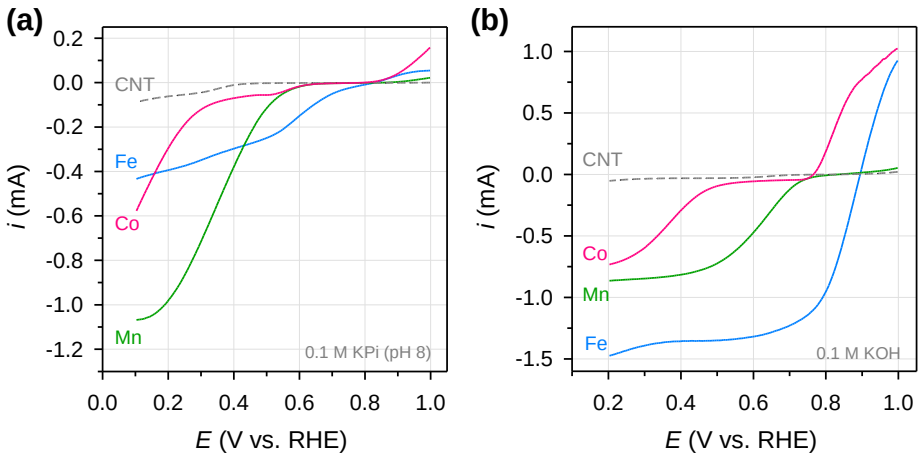

Fig. S23. Linear sweep voltammograms of MPc/CNT and CNT showing the hydrogen peroxide reduction reaction (HPRR) activity measured in (a) N_2-saturated 0.1 M KPi (pH 8) containing 5 mM H_2O_2 and (b) N_2-saturated 0.1 M KOH containing 5 mM H_2O_2.

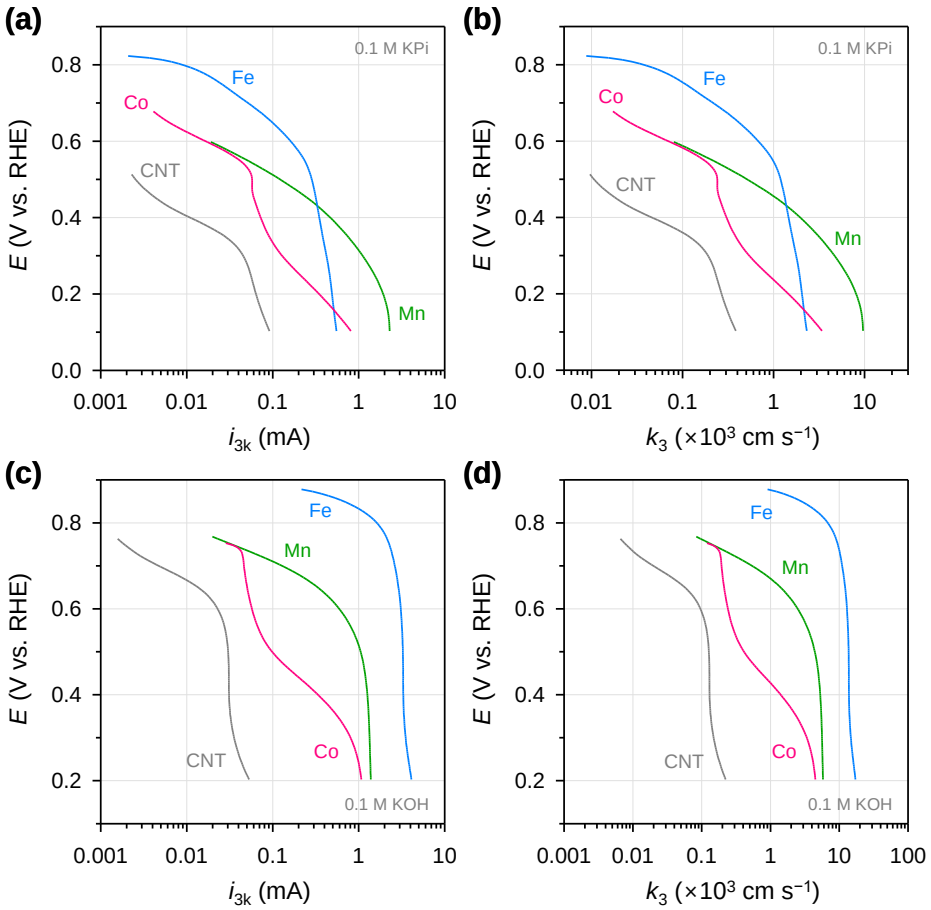

Fig. S24. (a) HPRR kinetic current (i_{3k}) of MPc/CNT and CNT in 0.1 M KPi (pH 8) and (b) the corresponding rate constant for the HPRR (k_3). (c) i_{3k} of MPc/CNT and CNT in 0.1 M KOH and (d) the corresponding k_3.

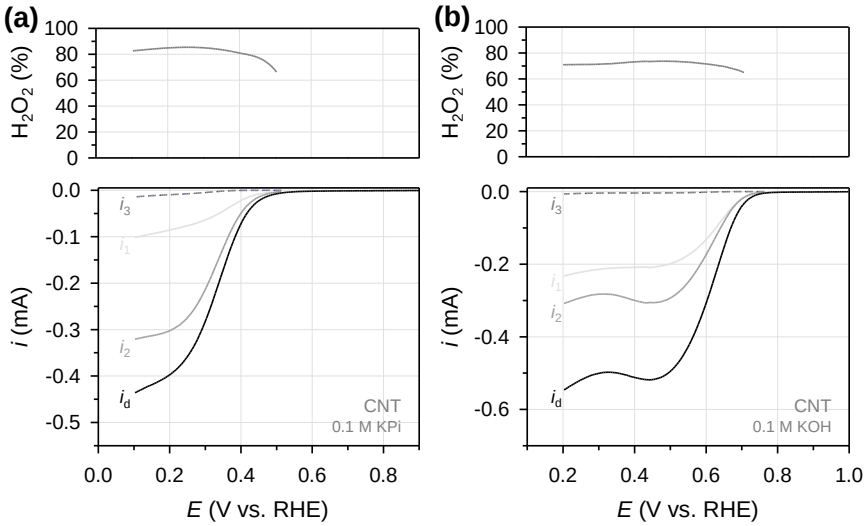

Fig. S25. The decoupled linear sweep voltammograms of CNT into i_1–i_3 and the H_2O_2 selectivity (H_2O_2 for short) analyzed in (a) 0.1 M KPi (pH 8) and (b) 0.1 M KOH.

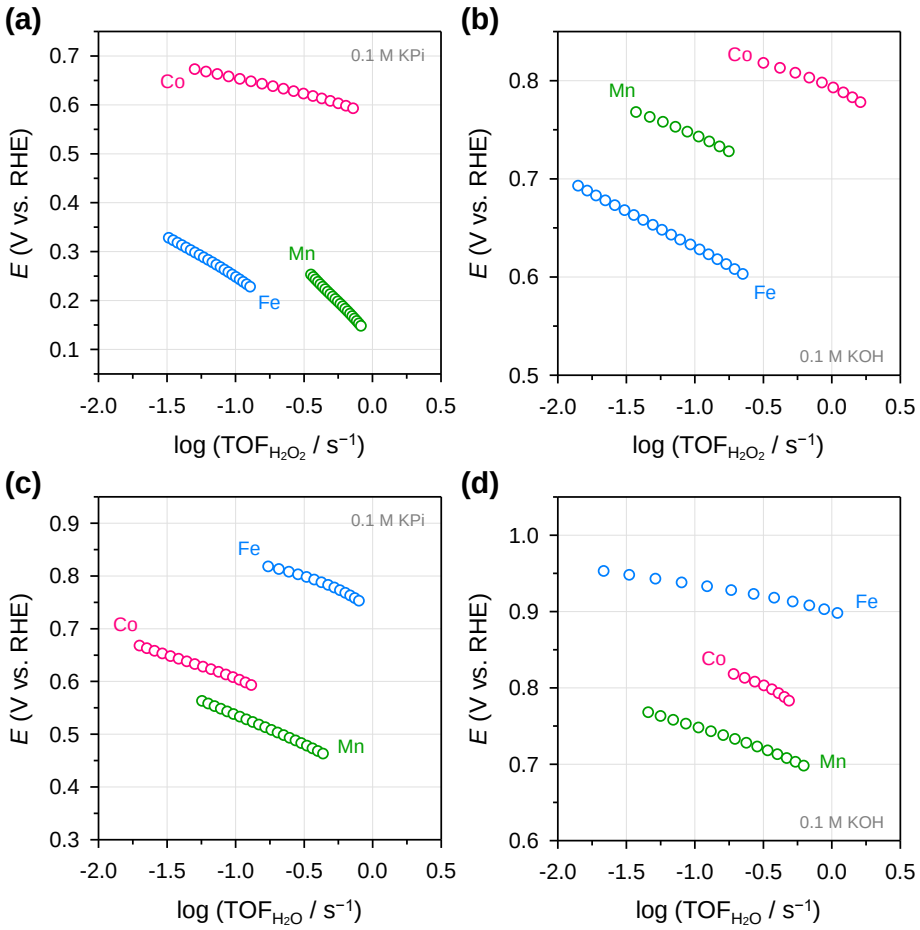

Fig. S26. Potential-dependent turnover frequency (TOF) per metal site of MPc/CNT for H_2O_2 generation ($2e^-$ ORR) in (a) 0.1 M KPi and (b) 0.1 M KOH. TOF for H_2O generation ($4e^-$ ORR) in (c) 0.1 M KPi and (d) 0.1 M KOH

Table S4. Summary of turnover frequency (TOF) for the $2e^-/4e^-$ ORR of CoPc/CNT and FePc/CNT compared with that of previously reported catalysts.

Catalyst	TOF (s^{-1})	*E* (V vs. RHE)	Electrolyte	Reference [c]
CoPc/CNT	0.6 [a]	0.60	0.1 M KPi (pH 8)	This work
CoPc/CNT	0.8 [a]	0.80	0.1 M KOH	This work
FePc/CNT	1.0 [b]	0.90	0.1 M KOH	This work
Co_1–NG(O)	3.38 [a]	0.65	0.1 M KOH	17
Co/NC	11.48 [a]	0.5	0.1 M PBS (pH 7)	55
CoN_4-PC	2.36 [a]	0.65	0.1 M KOH	56
Co-N/HPC	0.7 [a]	0.65	0.1 M KOH	57
3D-G-PFePc	0.93 [b]	0.9	0.1 M KOH	58
CoPc-Py-CNT	0.23 [b]	0.73	0.1 M NaOH	59

[a] TOF for the $2e^-$ ORR
[b] TOF for the $4e^-$ ORR
[c] Reference numbers referred in the main text

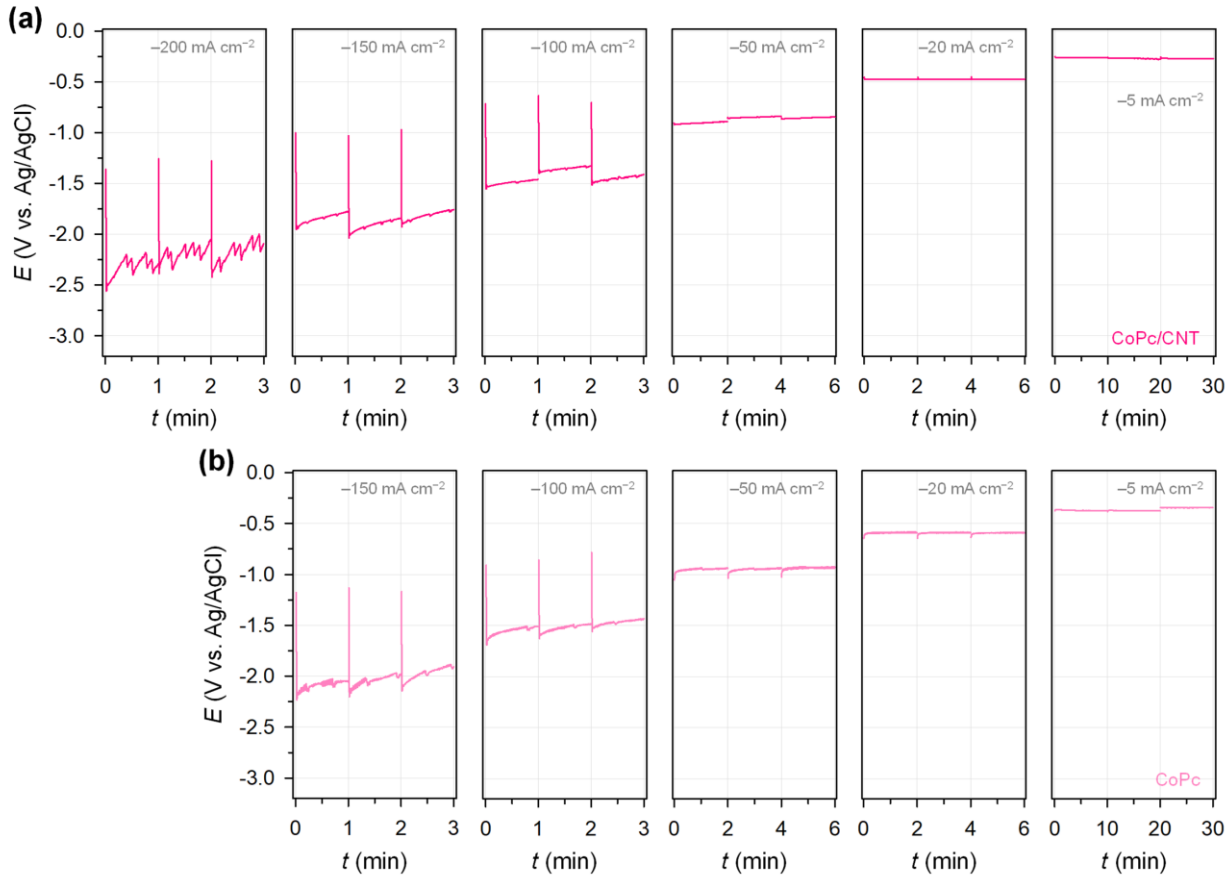

Fig. S27. Chronopotentiometry curves obtained at different current densities in a flow electrolyzer with (a) CoPc/CNT-based gas-diffusion electrode (GDE) and (b) CoPc-based GDE as the cathode. The electrolyte was 1 M KPi (pH 8).

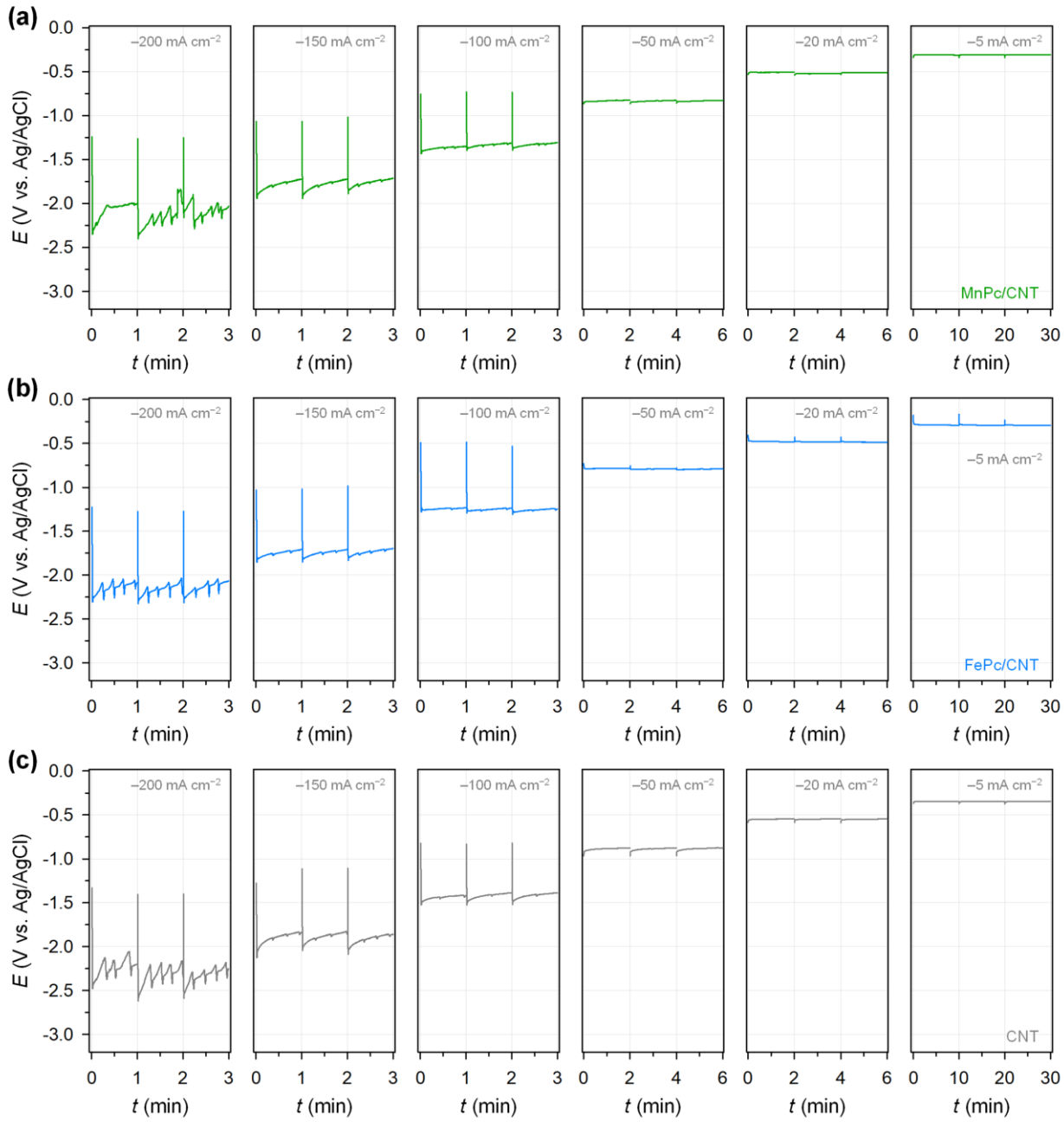

Fig. S28. Chronopotentiometry curves obtained at different current densities in a flow electrolyzer with (a) MnPc/CNT-based GDE, (b) FePc/CNT-based GDE, and (b) CNT-based GDE as the cathode. The electrolyte was 1 M KPi (pH 8).

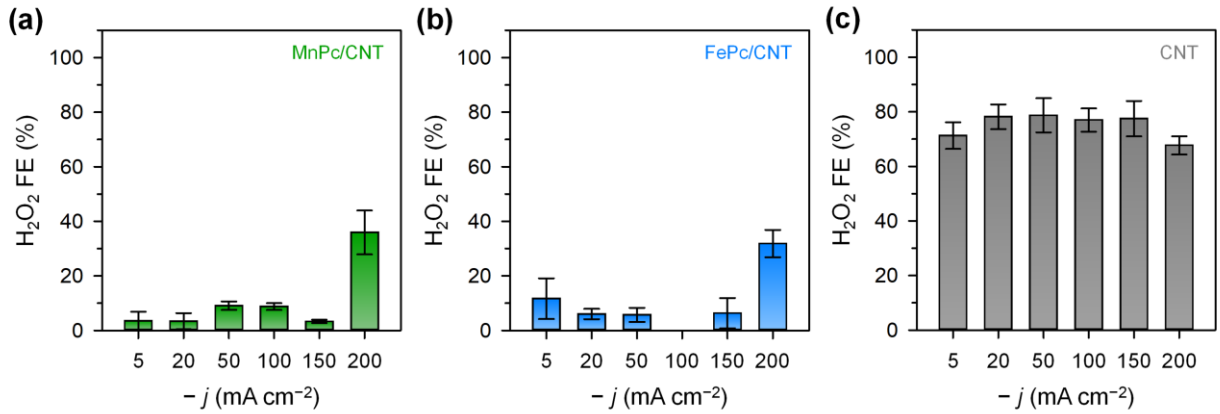

Fig. S29. H_2O_2 FE as a function of the current densities in the flow electrolyzer measurements with (a) MnPc/CNT-based GDE, (b) FePc-based GDE, and (c) CNT-based GDE as the cathode

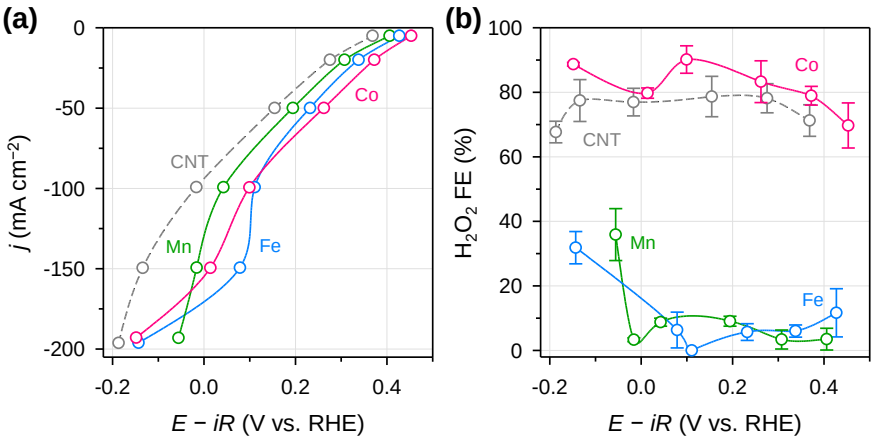

Fig. S30. (a) Current density and (b) H_2O_2 FE as a function of applied potentials in a flow electrolyzer with MPc/CNT- and CNT-based GDE as the cathode.

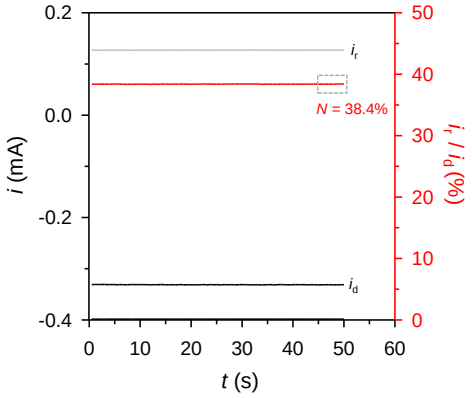

Fig. S31. Chronoamperometry curves measured using the catalyst-free rotating ring disk electrode as the working electrode in 2 mM $K_3[Fe(CN)_6]$ + 1 M KCl.

Table S5. The Gibbs free energy correction values for gas molecule and adsorbates.

(eV)		ZPE	$\int C_p\, dT$	$-TS$	**Sum**
Gaseous molecule	H_2	0.270	0.086	−0.403	−0.043
	H_2O	0.566	0.103	−0.673	−0.004
Adsorbate	O*	0.025	0.048	−0.013	0.190
	OH*	0.326	0.001	−0.001	0.326
	OOH*	0.393	0.048	−0.102	0.339